J. Electroanal. Chem., 144 (1983) 217–234
Elsevier Sequoia S.A., Lausanne – Printed in The Netherlands

ANODIC OXIDATION OF DIHYDRONICOTINAMIDE ADENINE DINUCLEOTIDE AT SOLID ELECTRODES; MEDIATION BY SURFACE SPECIES

ZDENEK SAMEC * and PHILIP J. ELVING

Department of Chemistry, The University of Michigan, Ann Arbor, MI 48109 (U.S.A.)

(Received 8th October 1981; in revised form 26th August 1982)

ABSTRACT

The mechanism and kinetics for the two-electron oxidation of 1,4-dihydronicotinamide adenine dinucleotide (NADH) to NAD^+ at gold, platinum and glassy carbon (GC) rotating disc electrodes at various solution pH and NADH concentrations can be rationalized in terms of the electron transfer occurring through mediator redox systems, located close to the electrode surface, such as the redox couples formed by oxygen-containing species adsorbed at Au and Pt surfaces. Analogous catalysis of NADH oxidation is provided by sulfide species adsorbed on a gold electrode surface. An important factor in differentiating the behavior of the three types of electrodes is the strong adsorption of NADH at Pt and Au, and of NAD^+ at GC. Since oxidation of adsorbed NADH starts at more positive potential than oxidation of bulk NADH, the latter occurs at Au or Pt electrode surfaces covered by adsorbed NADH, or at GC electrodes surfaces covered to some extent by adsorbed NAD^+. The theory for the surface EC catalytic mechanism is considered.

INTRODUCTION

The electrochemical oxidation of 1,4-dihydronicotinamide adenine dinucleotide (NADH) has been studied at glassy carbon (GC), pyrolytic graphite (PG) and platinum (Pt) electrodes from the viewpoints of analysis, role of the NAD^+/NADH redox couple in biological phenomena, and use of the couple in chemical and energy conversion processes (cf. refs. 1–5) **. It is well established that NADH undergoes in both aqueous and nonaqueous media an apparently single-step two-electron (2 e) oxidation [6–9] to enzymatically active NAD^+ [9,10] (cf. Fig. 1),

$$NADH \rightarrow NAD^+ + H^+ + 2\,e \qquad (I)$$

Some evidence has been presented which indicates the involvement of two successive 1 e steps [11], of a slow chemical deprotonation step [12] and of a second order

---

* Permanent address: J. Heyrovský Institute of Physical Chemistry and Electrochemistry, U továrven 254, 10200 Prague 10, Czechoslovakia.

** Although half-reactions and redox couples may be written or cited as both reductions and oxidations to indicate the direction of movement, potentials cited are consistent with the formulation as reductions, i.e., $Ox + n\,e = Red$.

pH-dependent chemical reaction [4]. The latter may be the dimerization or disproportionation of the intermediate radicals $NADH^+$ and $NAD^·$ [4].

Adsorption has been suggested [8,10,13] as a cause for catalytic and inhibition effects observed in the NADH oxidation, but only recently has evidence been presented [14–16] for an adsorption-controlled step. The possible role of oxide formation at GC electrodes has been noted [8,17]. The catalytic oxidation of NADH at GC or PG electrodes chemically modified by oxygen-containing functionalities has been reported [17,18].

The involvement of adsorption implies the need to control and to monitor the electrode surface carefully, before and during the electrochemical experiment [4,8]. The present study examines the correspondence between the rate of NADH oxidation at gold (Au), Pt and GC electrodes, and the state of the electrode surface as characterized electrochemically, as well as the mass-transport and charge-transfer kinetic characteristics of reaction (I).

EXPERIMENTAL

Chemicals

NADH, NAD^+, NMN^+ and ADPR (P–L Biochemicals), NMNH (Sigma), and AMP (Calbiochem) were pure enough to be used as received (cf. Fig. 1 caption for acronym glossary). Buffer solutions (pH 6.9, 8.2, 10.5) were 0.25 *M* in K_2SO_4 and 0.05 *M* in phosphate. Test solutions were deoxygenated before measurement by nitrogen bubbling.

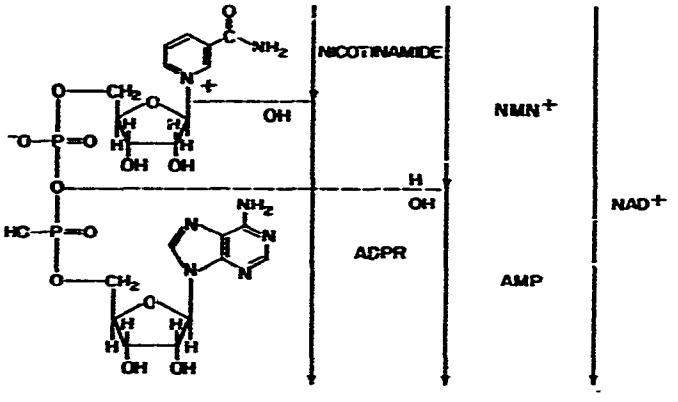

Fig. 1. Formula of enzymatically active β-nicotinamide adenine dinucleotide (NAD^+). Nicotinamide mononucleotide is designated by NMN^+, adenosine diphosphate ribose by ADPR, and adenosine 5'-monophosphate by AMP. Reduction (2 *e*; H^+) of NAD^+ and NMN^+ to NADH and NMNH, respectively, results in H addition at C(4) of the nicotinamide, bond shift and loss of quaternary character at N(1).

Apparatus

Electrochemical measurements were made with a Princeton Applied Research 170 multipurpose instrument and a three-compartment water-jacketed cell [19], kept at 25°, whose counter and reference electrode compartments were filled with background solution. A variable speed Caframo motor (1–40 rps) was used to rotate the electrodes.

Electrodes

Discs of 0.5 cm (GC) or 0.081 cm (Pt; Au) diameter were cemented into a glass tube (GC) or Teflon cylinder (Au) with an epoxy adhesive, or sealed into a soft glass tube (Pt). The geometric areas, determined by limiting current measurement for hexacyanoferrate(III) reduction at the RDE [20], were 0.169 cm^2 for GC and 5.0×10^{-3} cm^2 for Pt and Au. Potentials cited are referred to the saturated calomel reference electrode used. The counter electrode was a gold gauze.

Electrode pretreatment and real surface area

The electrode surfaces were first polished on rotating 600-mesh SiC paper. In order to obtain a clean reproducible surface, as indicated by a steady-state cyclic voltammogram [21] (Fig. 2), the (stationary) electrodes were scanned in the background solution between the onsets of hydrogen and oxygen evolution, e.g., at pH 6.9, between −0.6 and 1.35 V, −0.44 and 1.0 V, and −1.6 and 1.0 V for Au, Pt and GC, respectively; the polarization rate was 0.1 V s^{-1}, but Pt and Au were first scanned at 10 V s^{-1} for 10 min. This pretreatment was stopped on polarization towards more positive potential at a potential before the onset of oxygen adsorption or surface oxidation, which, at pH 6.9, is ca. −0.4, 0.1 and 0.7 V for GC, Pt, and Au, respectively, (Fig. 2) The start of oxygen adsorption on Au shifts negatively at ca. −60 mV/pH and the potential region of oxygen adsorption is broadened [22]; a similar pH effect seen with Pt [23–25] is connected with H^+ involvement in the adsorption process.

The actual Au electrode surface area was determined by measuring the charge consumed on oxygen adsorption in 0.5 *M* H_2SO_4 up to the I–E curve minimum at 1.45 V immediately before O_2 evolution (Fig. 2); this charge is independent of polarization rate and, based on comparison with BET surface area measurement, corresponds to 400 μC cm^{-2} of real surface area [26]. The area found of 0.042 cm^2 yields a roughness factor of 8.5.

The Pt electrode area was based on the charge consumed on adsorption of atomic hydrogen in the electrochemical reaction, $H^+ + e = H_{ads}$, in 0.5 *M* H_2SO_4 [21]; the generally accepted factor for monolayer and 1 : 1 Pt : H stoichiometry is 210 μC cm^{-2}. Evaluation from the voltammogram in 0.5 *M* H_2SO_4 (Fig. 2) [27] gave a real surface area of 0.039 cm^2 and a roughness factor of 7.8.

No standard method is available for determination of the real surface of the GC electrode.

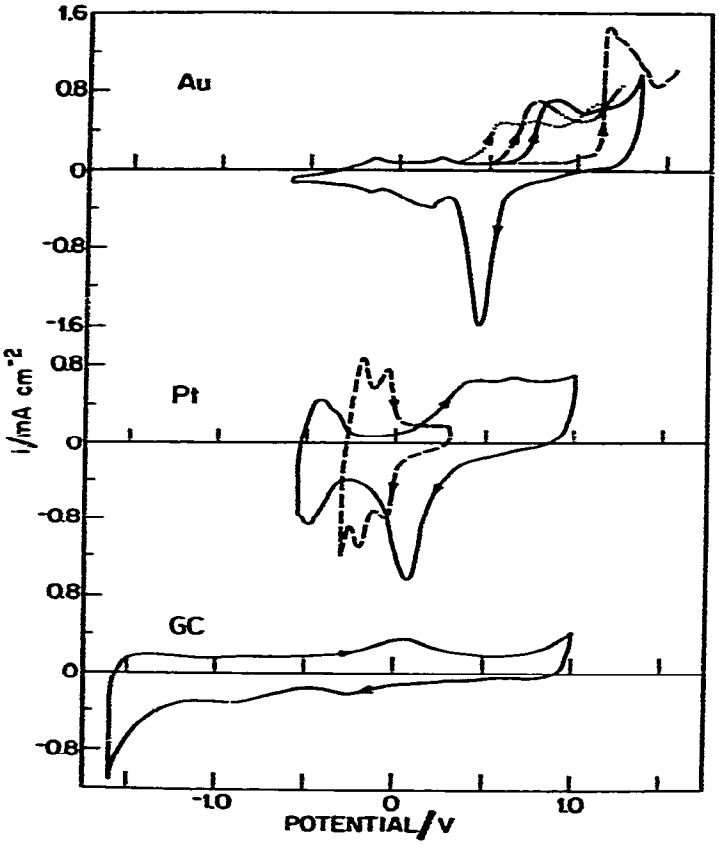

Fig. 2. Steady-state voltammograms at stationary Au, Pt and GC electrodes in buffered background electrolyte solutions (0.25 *M* K_2SO_4; 0.05 *M* phosphate buffer: pH 6.9 (———), 8.2 (-·-·-), 10.5 (·····)) and in 0.5 *M* H_2SO_4 (— — —). Rate of polarization: 0.1 V s^{-1}: arrowheads indicate the direction of the potential scan. Current density is based on the geometric electrode area.

RESULTS

Adsorption

Adsorption at Au and Pt electrodes has been examined by a dip technique.

After its electrochemical pretreatment, the Au electrode was removed from the cell and was dipped for 5 min in a 1 m*M* solution of NADH in the background solution, while rotated at 30 rps. In the blank experiment, the electrode was dipped in the background solution alone. The electrode was then thoroughly washed with water and redipped in the background solution in the cell. The cyclic voltammogram of a Au electrode after contact with NADH, starting at −0.6 V and reversing at

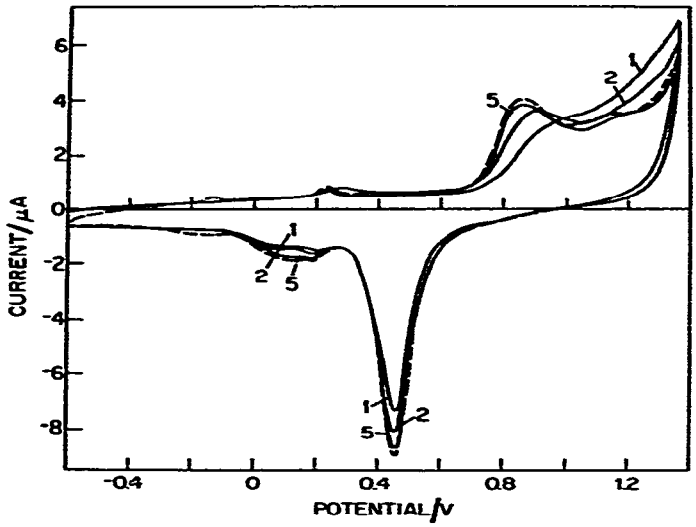

Fig. 3. Cyclic voltammograms at a stationary Au electrode covered by adsorbed NADH and immersed in pH 6.9 solution. Curves are labeled by serial number of repetitive voltage pulses (0.1 V s^{-1}) between −0.6 V (start) and 1.35 V. Dashed curve: steady-state cyclic voltammogram for a clean Au electrode.

1.35 V (Fig. 3), is characterized by the inhibition of oxygen adsorption in the 0.7 and 0.9 V region, increased anodic current between 1.0 and 1.35 V, and the need for at least 10 voltage scans in order to regain the voltammogram of the clean electrode.

The increased anodic current positive to 1.0 V may be due to simultaneous adsorbate oxidation and oxygen adsorption. These two phenomena can be separated by integration of the cyclic voltammogram on the basis that, in contrast to adsorbate oxidation, the contribution of oxygen adsorption to charge consumption, Q^+, on the scan from −0.6 to 1.35 V is balanced by the adsorbed oxygen reduction contribution to charge consumption, Q^-, on the return scan. Thus, the charge yield, $Q_n = Q_n^+ - Q_n^-$, at −0.6 V on the n-th voltage pulse would represent only the charge consumed in adsorbate oxidation. However, integration of the clean electrode steady-state voltammogram yields some oxidation charge, which may correspond to Au dissolution [28], charge lost in the O_2 evolution, and/or incomplete adsorbed oxygen reduction. Since the possible influence of adsorbed species on Au dissolution and O_2 evolution rates is not known, one can only assume that the unbalanced oxidation charge connected with these processes in presence of adsorption is essentially the same as for the clean electrode. Therefore, the charge consumed on adsorbate oxidation is calculated by subtracting Q_n for the clean electrode from that for the electrode covered by adsorbate.

In order to isolate the influence, particularly on adsorption, of the component entities in NADH, the following compounds (Fig. 1) were also examined: NAD^+, NMN^+ and NMNH in which the elements of AMP have been removed from

TABLE I

Characterization of magnitude of adsorbed layers on gold electrodes

Compound[a]	Q_T^{ox}/e.p.s.[b]	$\Delta Q_0/Q_0^0$[c]
Blank	0.4	0.10
NADH	1.6	0.55
NAD^+	1.4	0.68
NMNH	0.9	0.30
NMN^+	1.1	0.32
AMP	1.9	0.70
ADPR	1.2	0.35

[a] Presumed adsorbate after exposure of electrode to compound specified.

[b] Limiting total oxidation charge Q_T^{ox} of adsorbed layer, i.e., integration of charges for all pulses which are necessary before the steady-state cyclic voltammograms for a clean electrode is obtained (cf. text for method of determination).

[c] Relative decrease in oxygen adsorption $\Delta Q_0/Q_0^0$ between 0.7 and 0.9 V, which is a relative measure of the extent of adsorption on the electrode. Because of the difficulty in measuring the change in surface coverage at Au with adsorbate concentration, it is not clear whether the numbers obtained represent maximum coverage or an intermediate coverage reflecting the differences in energy of adsorption of different compounds adsorbed at the same bulk concentration.

NAD^+ and NADH; AMP; and ADPR in which the nicotinamide moiety has been removed from NAD^+ and NADH. Despite these structural differences, Au electrodes exposed to solutions of NADH, NAD^+, NMNH, NMN^+, AMP, or ADPR, exhibit voltammetric behavior qualitatively similar to that described in the two previous paragraphs.

The integrated charge, presumably due only to adsorbate oxidation, approaches a limiting value after 5 scans (NADH, NAD^+ and their components) or one scan (blank experiment), which represents the total charge, Q_T^{ox}, necessary for adsorbed layer oxidation (Table 1). The latter can be expressed as the number of electrons per surface gold atom (e.p.s.). The experimental factor of 400 $\mu C\ cm^{-2}$ for conversion of charge to e.p.s. (cf. previous section) is very close to that expected for an adsorbed monolayer with 1:1 Au:O stoichiometry [21] and thereby can be taken as the equivalent of 2 e.p.s. consumed in a surface charge-transfer reaction.

The extent of adsorption can be characterized by the relative decrease in oxygen adsorption between 0.7 and 0.9 V on the first scan from −0.6 to 1.35 V (Fig. 3), i.e., ratio decrease in charge consumed, Q_0^0, for the clean electrode (Table 1).

A cyclic voltammogram of a Pt electrode immersed in the background solution after its contact with 1 m*M* NADH also exhibits the inhibition of the electrochemical oxygen adsorption and several voltage scans are necessary for complete adsorbed layer oxidation. However, measurement of the charge consumed on adsorbed NADH oxidation is not reliable, mainly due to the tendency of Pt to adsorb O_2 from the air, to which the electrode is necessarily exposed by the dip technic. Q_T^{ox} is roughly twice as large as that for oxidation of NADH adsorbed on Au.

Because no charge transfer occurs between −0.55 and 0.0 V at Pt in the presence of NADH in solution, except for deposition or stripping of adsorbed atomic hydrogen, the extent of NADH adsorption can be estimated from the decrease in in situ atomic hydrogen adsorption. Surface coverages are 70, 73, 78, 79 and 79% for 0.2 m*M* and 76% for 0.4, 1.0 and 1.9 m*M*. Thus, NADH adsorption at Pt increases slightly with bulk NADH concentration.

NADH oxidation at rotating disc electrodes

Electrode pretreatment in pH 6.9 buffer was stopped at −0.6 (GC), 0.0 (Pt) or 0.6 (Au) V; the solution was replaced by one containing NADH. After deoxygenation, a slow scan (2 mV s^{-1}) towards more positive potential was applied. The wave recorded on both positive and negative polarization was corrected for background current (Fig. 4), using for Pt and Au the voltammograms for electrodes covered by adsorbed NADH. When the polarization was stopped in either direction, the NADH oxidation current changed negligibly (< 10%) during 5 min, indicating that the wave on both positive and negative polarization at Pt and Au has the stationary character, or, at least, corresponds to the particular electrode surface state, which changes markedly after potentials close to onset of O_2 evolution are reached (cf. hysteresis of anodic waves in Fig. 4).

At 2 m*M* or less NADH, the limiting current, I_l, for all three electrodes is linearly dependent on $\omega^{1/2}$ (angular velocity $\omega = 2\pi f$; f in rps) and independent of scan direction. Above 2 m*M*, a decline from linearity towards lower values is seen as f approaches 30 rps. At Pt and Au electrodes, I_l is constant between pH 6.9 and 10.5. When I_l is related to the geometric electrode area, A, all points in Fig. 5 practically

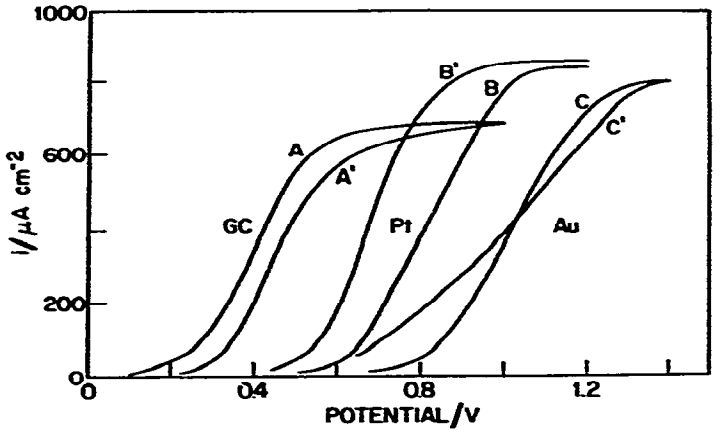

Fig. 4. Anodic wave of NADH at pH 6.9 corrected for background current at GC (A, A'), Pt (B, B') and Au (C, C') rotating disc electrodes, recorded on positive (A, B, C) and negative (A', B', C') potential scan (2 mV s^{-1}). Rotation speed: 30 rps; NADH concentration: 1 m*M* (GC) and 1.1 m*M* (Pt, Au).

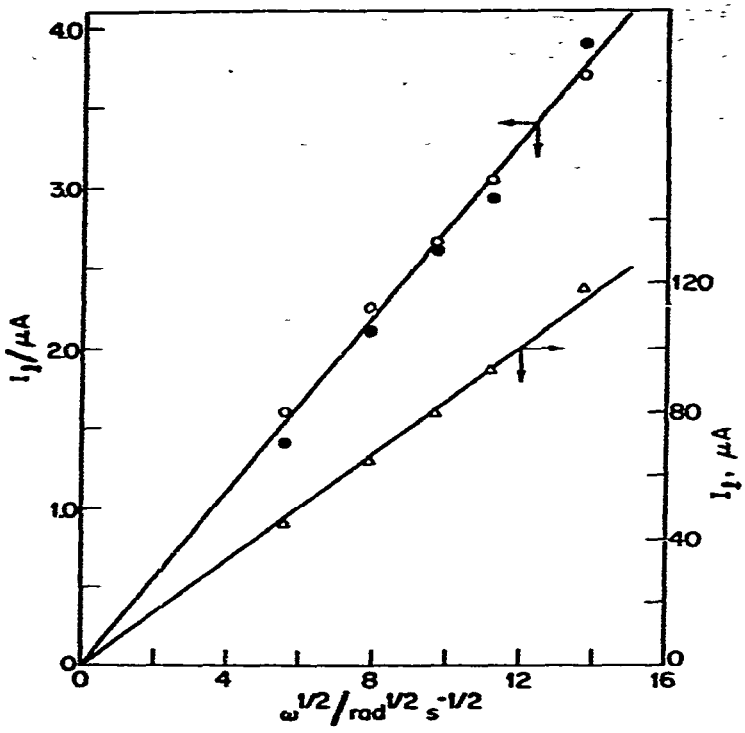

Fig. 5. Dependencies of the limiting current, I_l, for the anodic wave of NADH (1 mM) at pH 6.9 on the square root of the angular velocity, ω, for Au (○), Pt (●) and GC (△) rotating disc electrodes.

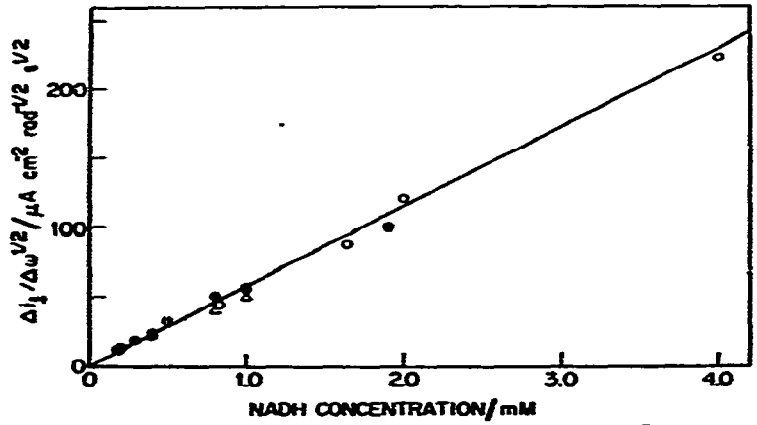

Fig. 6. Dependency of the slopes of plots of the limiting current density, i_l, vs. square root of the angular velocity, ω, on bulk NADH concentration at pH 6.9 for rotating electrodes of Au (○), Pt (●) and GC (△): i_l is the ratio of limiting current, I_l, to geometric electrode area. The slope of the line is 57.5 A cm $rad^{-1/2}\ s^{1/2}\ mol^{-1}$.

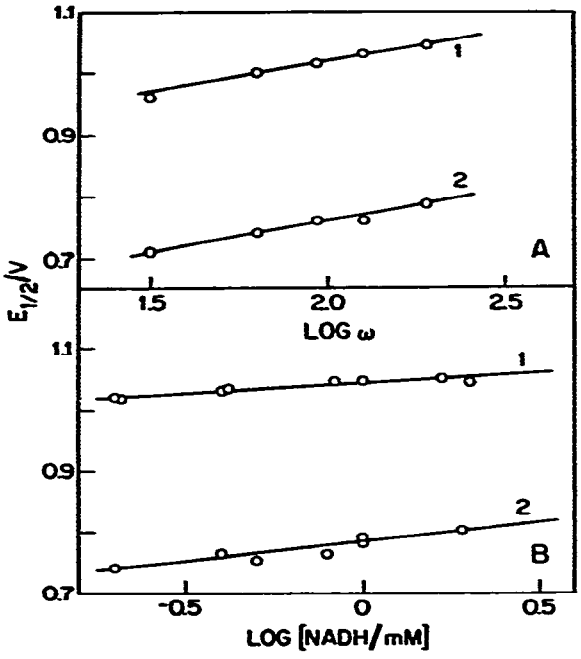

Fig. 7. Dependencies of $E_{1/2}$ for NADH at pH 6.9 on (A) electrode rotation speed, ω, at 1 m*M* NADH and (B) bulk NADH concentration at 30 rps. Rotating disc electrodes: 1, Au; 2, Pt.

fall on a single straight line. This is seen in the linear plot of the $I_l/\omega^{1/2}$ ratio, normalized for *A*, vs. NADH concentration (Fig. 6).

With increasing *f* or NADH concentration, the wave at Pt and Au RDE shifts positively (Fig. 7); $\Delta E_{1/2}/\Delta(\log \omega)$ is 109 (Au) and 104 (Pt) mV; $\Delta E_{1/2}/\Delta(\log c)$ is 33 (Au) and 66 (Pt) mV. On the other hand, the wave shifts negatively with increasing pH and the reciprocal slope of the $\log[I(I_l - I)^{-1}]$ vs. *E* plot decreases (Table 2); $\Delta E_{1/2}/\Delta$ pH = −53 (Au) and −28 (Pt) mV.

TABLE 2

Half-wave potentials and log plot slopes[a] for the NADH oxidation wave at rotating disc electrodes[b]

Electrode	$E_{1/2}$ (Slope)/V		
	pH 6.9	pH 8.2	pH 10.5
Au	1.02 (0.19)	0.96 (0.19)	0.83 (0.11)
Pt	0.82 (0.16)		0.72 (0.13)
GC	0.40 (0.17)		

[a] The slopes given in parentheses are the reciprocal slopes in V for plots of $\log[I(I_l - I)^{-1}]$ vs. *E*.
[b] Electrodes were rotated at 30 rps while being polarized towards more positive potential at 2 mV s^{-1}.

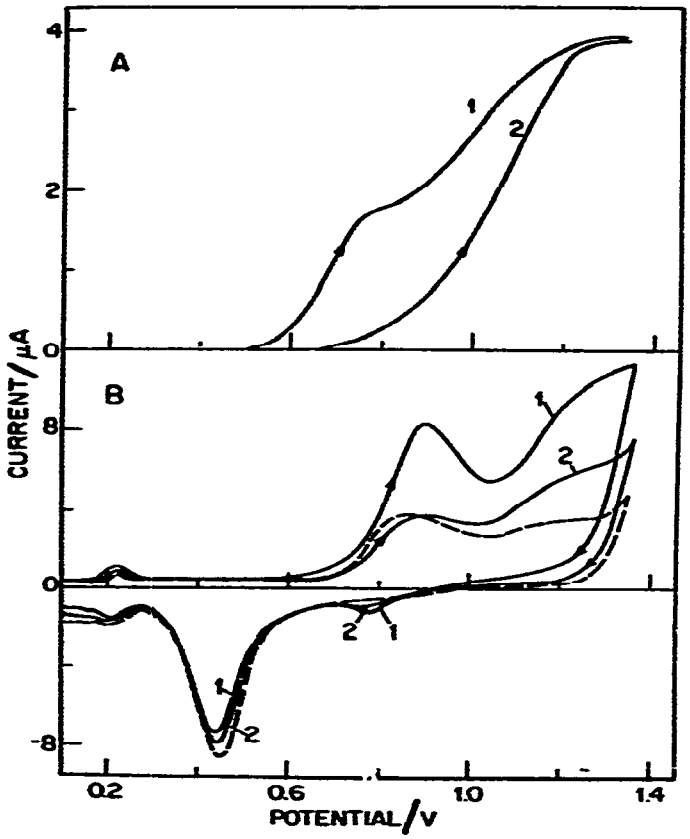

Fig. 8. (A) Anodic wave of NADH (1 m*M*) at a Au rotating disc electrode (30 rps) covered by adsorbed sulfide species (polarization rate = 2 mV s^{-1}) and (B) cyclic voltammograms (0.1 V s^{-1}) at a stationary Au electrode covered by adsorbed sulfide species (solid line) or at the clean electrode (dashed line). pH = 6.9. Curves are labeled by the serial number of the repetitive voltage pulse between (A) 0.4 and 1.35 V and (B) −0.6 and 1.35 V. Arrowheads indicate the direction of the potential scan.

Effect of adsorbed sulfide at Au

Sulfide was adsorbed at a Au surface by the dip procedure described above (dipped for 2 min in 1 *M* Na_2S in pH 6.9 buffer). On cyclic voltammetry of the covered stationary electrode (Fig. 8B), anodic peaks appear at ca. 0.9 and 1.2 V on the first voltage scan; on subsequent pulses, the more positive peak decreases. At least 10 scans are needed to obtain the clean electrode steady-state voltammogram; Q_T^{ox} on oxidation of the adsorbed sulfide layer is 7.8 e.p.s. When the first scan is reversed at 1.0 V and the range is extended to 1.35 V on subsequent scans, Q_T^{ox} is 2.0 e.p.s. for the first scan and 7.2 e.p.s. for all subsequent, necessary scans.

The effect of adsorbed sulfide on the NADH oxidation was examined as follows. The anodic wave was recorded as usual (cf. Fig. 4C); the electrode was polarized to −0.6 V, removed, washed with distilled water, dipped in 1 *M* Na_2S in base electrolyte for 2 min while rotated at 30 rps, removed, washed with distilled water, returned to the NADH solution in the cell, and polarized to −0.6 V; the NADH wave was recorded at 2 mV s^{-1} towards more positive potential starting at 0.4 V (Fig. 8A; curve 1). The NADH oxidation is appreciably catalyzed below 0.8 V; at more positive potential, the wave is close to that recorded on Au not covered by sulfide; on repeated scans between 0.4 and 1.35 V, the wave (Fig. 8A; curve 2) practically coincides with that on uncovered Au. When the sulfide covered electrode is polarized by repetitive scans between 0.4 and 0.675 V, the catalyzed NADH oxidation proceeds without a change in rate.

Logarithmic analysis of both waves in Fig. 8A indicates that the catalytic effect of adsorbed sulfide is accompanied by a change in the reciprocal of the $\log[I(I_l - I)^{-1}]$ vs. E plot at the wave foot from 190 to 115 mV. Repetition of the experiment at 0.2 to 1.0 m*M* NADH showed no effect on the log plot slope at the wave foot. However, the latter shifts positively with increasing NADH concentration: $\Delta E_{1/2}/\Delta(\log c) = 55$ mV.

DISCUSSION

Adsorption

The data indicate that the compounds examined are strongly and irreversibly adsorbed at the gold surface. The compounds lacking the adenine moiety, i.e., NMNH and NMN^+, are adsorbed at Au to a lesser extent than those having that moiety (Table 1). The difference between AMP and ADPR is understandable in terms of the increased number of hydrophilic groups in ADPR. If surface coverage reflects the relative strength of bonding to the surface, the adenine moiety is the preferential site for NADH and NAD^+ adsorption at Au and, possibly, Pt. This is in full agreement with the conclusion drawn by Takamura et al. [29], from their specular reflectivity measurements of adsorption of NAD^+, NMN^+, nicotinamide, adenine and adenosine at Au electrode surfaces. Adenine is considered to be the adsorption site for NAD^+ at Hg [3] and GC [16] electrodes. The appreciable adsorption of NMNH and NMN^+, however, points to the pyridine moiety possibly being also involved in adsorption at Au.

Inspection of the space-filling model [30] of NADH shows that the estimated minimum projected area for the folded molecule to planes perpendicular or parallel to that of the adenine and pyridine rings is ca. 0.85 nm^2 or 1.25 nm^2, respectively; the minimum projected area for the flat open molecule is 1.90 nm^2. Since the area per one surface atom of polycrystalline gold is much less, i.e., 0.087 nm^2, it is probable that more than one surface atom is blocked by a single adsorbed NADH molecule. Consequently, unless NADH is adsorbed in a multilayer, the oxidation charge Q_I^{ox} of 1.6 e.p.s. certainly corresponds to more than 2 electrons consumed in

the oxidation of one adsorbed NADH molecule. The same should hold for the other adsorbates listed in Table 1.

While data indicate that NADH is strongly adsorbed at a Pt or Au electrode surface, it is, in contrast, only weakly adsorbed at GC as compared with the strong adsorption of NAD^+ at GC from solution or in the electrochemical step [14–16],

$$NADH \rightarrow NAD^+_{ads} + H^+ + 2e \qquad (II)$$

The effect of successive voltage scan oxidation of the adsorbed layer at Pt and Au parallels that for NAD^+ adsorption at GC (eqn. (II)) [14–16], the only difference being that in the former case the adsorbed layer is gradually removed by repetitive scanning while in the latter case it is gradually formed. In general, the behavior of the adsorbed layer at Pt and Au can be accounted for on the basis that, as oxidation of adsorbed species occurs close to the onset of O_2 evolution, limitation of the available potential range by the latter process may not allow the positive potentials necessary for adsorbate oxidation to be reached in a single voltage scan excursion.

From the high charge consumption on adsorbate oxidation and the small differences in adsorption and oxidation between NADH and NAD^+, and NMNH and NMN^+, we can conclude that NADH participates in two different oxidation processes at Au and Pt electrodes. The first process, described by reaction (I) gives rise to the 2 e anodic wave (Fig. 4); the second can be described by

$$NADH \rightarrow (NADH)_{ads} \rightarrow X + n\,e \qquad (III)$$

Because oxidation of adsorbed NADH obviously starts at more positive potential than reaction (I), the latter occurs at an electrode surface covered by adsorbed NADH, when a Au or Pt electrode is polarized by a positive potential sweep. At GC, the electrochemical adsorption (reaction (II)) occurs in place of reaction (III) so that reaction (I) occurs at a surface covered to some extent by adsorbed NAD^+.

Mediated mechanism of NADH oxidation

Unlike NAD^+ reduction at a Hg electrode, NADH oxidation at solid electrodes is much less informative about the mechanism of the overall reaction (I). In the former case, the data are best explained by a sequence of two 1 e steps [2],

$$NAD^+ + e \rightleftarrows NAD^{\cdot} \qquad (IV)$$

$$NAD^{\cdot} + H_3O^+ + e \rightarrow NADH + H_2O \qquad (V)$$

accompanied by dimerization of the intermediate free radical,

$$2\,NAD^{\cdot} \rightarrow (NAD)_2 \qquad (VI)$$

The rate constant for charge–transfer reaction (IV) probably exceeds 1 cm s^{-1} [13]; that for charge–transfer reaction (V) has not yet been evaluated. Since the irreversible polarographic wave corresponding to reaction (V) occurs at potentials as negative as -1.6 V, reaction (V) is rather slow. The rate constant for dimerization reaction (VI) is of order of $10^6\ M^{-1}\ s^{-1}$ [2].

If the sequence of steps (IV) and (V) is reversed on NADH oxidation, reaction (V) can be assumed to be rate-determining. Since the oxidation occurs positive to 0.2 V (Fig. 4), oxidation of $NAD^{\cdot}$ to NAD^{+} would be sufficiently rapid to outrun the dimerization (reaction (VI)), so that practically no dimer is produced. Under these circumstances, a single anodic 2 *e* wave should be observed, which corresponds to the irreversible 1 *e* NADH oxidation (reaction (V)) and which is independent of the nature of electrode material, NADH concentration and solution pH as well. However, since all three effects are involved in NADH oxidation at solid electrodes, modification of the mechanism outlined is required. The effect of electrode material is obviously most significant and it may underlie the effects of both NADH concentration and solution pH.

The correspondence between the rate of NADH oxidation at solid electrodes and the state of the electrode surface can be reasonably explained on the basis of intimate involvement of surface oxygen species in the rate-determining step of overall reaction (I), i.e.,

$$NADH + H_2O \rightarrow NAD^{\cdot} + H_3O^{+} + e \qquad \text{(VII)}$$

Such correspondence was first suggested by Blaedel and Jenkins [8].

The possible involvement of two surface oxygen redox systems in NADH oxidation is schematically depicted in Fig. 9. The electron–transfer path involves electron exchange between energy levels located at the surface oxygen atom and in the electrode, coupled with electron exchange between energy levels of the surface oxygen atom and the solution species, i.e., NADH molecule. The proton transfer path involves transfer of the proton bound to *C*(4) of NADH to a third species, which is the proton acceptor, e.g., H_2O, with possible intermediate formation of a bond to the surface oxygen atom:

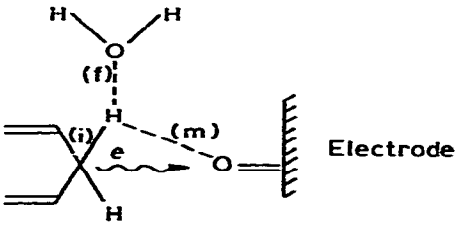

where i, f and m designate the initial, final and possible intermediate bonds, respectively, of the transferred proton.

Thus, two mechanisms can be envisaged for the proton transfer path. In one, electron transfer through the intermediate state located close to the surface oxygen atom and proton transfer are decoupled from each other, i.e., the proton bound to C(4) of NADH is not involved in the activated complex formed before electron transfer may occur. The stable intermediate state in the electron–transfer path, which may be but need not be actually formed, would be represented by $NAD^{\cdot}H^{+}$ and $O_{ads}(OH^{\cdot}_{ads})$. Subsequently, the proton is transferred from $NAD^{\cdot}H^{+}$ to a proton acceptor in a distinct chemical step, as supported by previous results [12].

In the second mechanism, a bond is formed between the transferred proton and the surface atoms, and the intermediate state in the electron–transfer path would be represented by NAD$^{\bullet}$ and $OH^{\bullet}_{ads}(H_2O)$. In order that the "inner-bridge" activated complex be formed, reorganization of the proton configuration with respect to both C(4) and surface oxygen atoms and proton acceptor is necessary.

On the whole, irrespective of whether or not a stable intermediate state is actually formed, electron transfer through a mediator energy level may represent a path which is kinetically more favorable than direct electron transfer.

The hypothesis that oxidation of NADH may proceed through different mediator redox systems located close to the electrode surface is further supported by the catalysis of NADH oxidation by surface-attached quinones [17] and by sulfide adsorbed at a Au electrode.

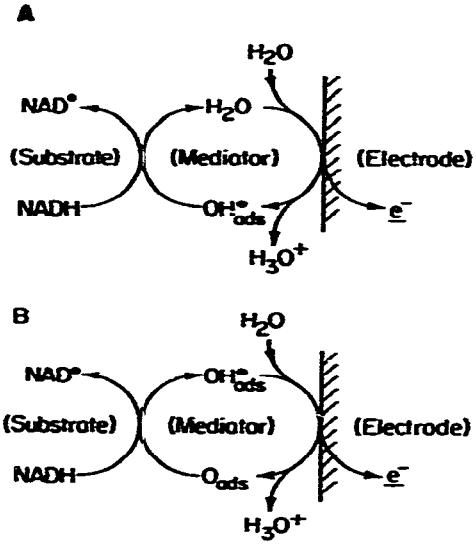

Fig. 9. Schematic depictions of possible surface oxygen redox systems as mediators in the oxidation of NADH at electrodes. A: OH_{ads}/H_2O redox couple. B: O_{ads}/OH_{ads} redox couple.

At pH 6.9, sulfide species adsorbed on Au are probably H_2S and HS^- (pK_a for H_2S: 7.04, 11.96). The charge of 7.8 e.p.s. consumed on total oxidation of the adsorbed sulfur layer indicates oxidation to the highest normal oxidation stage. Oxidation of the layer "by parts" reveals that the anodic peak at ca. 0.9 V (Fig. 8E) is due to 2 e oxidation to $S^{(0)}$ and that the peak at ca. 1.2 V is due to further oxidation to SO_4^{z-} (cf. ref. 31).

Significant catalysis of NADH oxidation at a Au electrode covered by adsorbed sulfur species (Fig. 8A) is associated exclusively with species in the lowest oxidation stage: H_2S_{ads} or HS^-_{ads}. In fact, the NADH wave on repeated slow potential scan

between 0.4 and 1.35 V (Fig. 8A; curve 2) practically coincides with that at a Au electrode not covered by sulfur species, although $S^{(0)}$ species are still present on the surface (Fig. 8B; curve 2). Furthermore, if a Au electrode covered by H_2S_{ads} or HS^-_{ads} is not polarized more positive than 0.68 V, at which oxidation of these species starts, the catalyzed NADH oxidation proceeds without significant time decay.

Such catalysis can be interpreted in terms of the involvement of such surface redox systems as $HS^{\cdot}_{ads}/HS^-_{ads}$ or $HS^{\cdot}_{ads}/H_2S_{ads}$ in the electron transfer from NADH to electrode in the same way as such surface redox systems as $O_{ads}/OH^{\cdot}_{ads}$. As the formal potentials of the $HS^{\cdot}_{ads}/H_2S_{ads}$ and $HS^{\cdot}_{ads}/HS^-_{ads}$ systems are probably less positive than that of the $O_{ads}/OH^{\cdot}_{ads}$ system, the oxidation of NADH is easier when the former systems are involved.

Theory for mediated mechanism

With the reference to Fig. 9, the surface EC catalytic mechanism will be considered,

$$Q_{ads} + H^+ + e \rightleftarrows QH_{ads} \qquad \text{(VIII)}$$

$$Q_{ads} + NADH \rightarrow QH_{ads} + NAD^{\cdot} \qquad \text{(IX)}$$

where Q_{ads}/QH_{ads} is the surface mediator redox couple. Such mechanism has been currently used to interpret the charge-transfer kinetics at chemically modified electrodes [32]. Some consequences arising from this type of mechanism for rotating disc electrode voltammetry have been analyzed [33].

Under stationary conditions, the surface concentrations Γ_Q and Γ_{QH} of Q and QH, respectively, do not vary with time, i.e.,

$$\partial\Gamma_Q/\partial t = k_{ox}\Gamma_{QH} - k_{ox}P^{-1}\Gamma_Q - k_c\Gamma_Q c^*_{NADH} = 0 \qquad (1)$$

where k_{ox} is the potential-dependent anodic rate constant, k_c is the rate constant of the chemical step (reaction (IX)), c^*_{NADH} is the NADH concentration at the electrode surface and P is the potential-dependent function

$$P = \exp[(F/RT)\cdot(E - E^{\theta})] \qquad (2)$$

Since the electrolyte solution is buffered, the proton concentration $c^0_{H^+}$ may be assumed to be constant throughout the solution space; it is included in the formal potential E^{θ} for electrochemical step (VIII),

$$E^{\theta} = E^0 + (RT/F)\ln c^0_{H^+} \qquad (3)$$

In eqn. (1), the principle of detailed balancing [34] is used to interrelate the cathodic (k_{red}) and anodic (k_{ox}) rate constants, $k_{red} = k_{ox}P^{-1}$.

Taking into account the fast follow-up oxidation of $NAD^{\cdot}$ to NAD^+, the diffusion current I is given by

$$I = (2FAD/\delta)(c^0_{NADH} - c^*_{NADH}) \qquad (4)$$

where A is the interfacial area, D is the diffusion coefficient of NADH, c^0_{NADH} is the

bulk NADH concentration and δ is the thickness of the diffusion layer,

$$\delta = 1.61\omega^{-1/2}\nu^{1/6}D^{1/3} \tag{5}$$

where ω is the angular velocity and ν is the kinematic viscosity.

Assuming that

$$\Gamma_Q + \Gamma_{QH} = \Gamma_0 = \text{constant} \tag{6}$$

a quadratic equation can be derived for the surface concentration Γ_Q:

$$p^2 + p\left[s_c + s_{ox}P(1+P)^{-1} - P(1+P)^{-1}\right] - s_cP(1+P)^{-1} = 0 \tag{7}$$

where $p = \Gamma_Q/\Gamma_0$ and the dimensionless kinetic parameters s_c and s_{ox} are defined as

$$s_c = D/k_c\,\delta\Gamma_0 \tag{8}$$

$$s_{ox} = Dc^0_{NADH}/k_{ox}\,\delta\Gamma_0 \tag{9}$$

Finally, the current I is given by

$$I = pI_d(s_c + p)^{-1} \tag{10}$$

where the limiting diffusion current I_d is

$$I_d = (2FAD/\delta)c^0_{NADH} \tag{11}$$

Two limits of eqn. (7) can be distinguished. First, when the surface charge transfer is very fast so that $k_{ox} \to \infty$ or $s_{ox} \to 0$ (the reversible case), eqn. (7) becomes [33]

$$p = P(1+P)^{-1} \tag{12}$$

In this case, the limiting current I_l is given by

$$I_l = I_d(1+s_c)^{-1} \tag{13}$$

and the half-wave potential, $E^{rev}_{1/2}$, is given by

$$E^{rev}_{1/2} = E^{\theta} + (RT/F)\ln s_c(1+s_c)^{-1} \tag{14}$$

On the other hand, when the surface charge transfer is very slow (the irreversible case), quadratic eqn. (7) remains to be solved. However, due to the kinetic overpotential, $P(1+P)^{-1} \to 1$ and

$$p^2 + p(s_c + s_{ox} - 1) - s_c = 0 \tag{15}$$

The limiting current is again given by eqn. (13), but the half-wave potential depends on the kinetic parameters of the electrochemical step (VIII). If, formally,

$$k_{ox}(E) = k^0_{app}\exp\left[(1-\alpha)F(E-E^0)/RT\right] \tag{16}$$

where k^0_{app} is the apparent rate constant and α is the apparent cathodic charge transfer coefficient, the half-wave potential is given by

$$E^{irr}_{1/2} = E^0 + \frac{RT}{(1-\alpha)F}\ln\left[\frac{Dc^0_{NADH}}{k^0_{app}\,\delta\Gamma_0}\cdot\frac{2s_c+1}{2(s_c+1)^2}\right] \tag{17}$$

On the basis of this theory, we can make the following generalizations about the electrochemical oxidation of NADH at solid electrodes.

(1) Because the limiting current I_l for the NADH wave is proportional to bulk concentration and $\omega^{1/2}$, and independent of pH and electrode material, we can conclude that it is controlled solely by diffusion of NADH to the electrode surface. Recalling eqns. (13 and 8), this means that $D/k_c\,\delta\Gamma_0 \ll 1$. Using then this relation and eqn. (5) for δ, a NADH diffusion coefficient of 3.3×10^{-6} cm^2 s^{-1} is calculated from the straight line slope in Fig. 6, which value is comparable to that calculated for NAD^+ from its DME reduction (3.4 or 4.3) $\times 10^{-6}$ cm^2 s^{-1} [2].

(2) As is apparent from eqns. (14 and 17), the nature of the electrode material may be reflected in the half-wave potential of the NADH wave through the formal potential E^{θ} of the surface redox couple (reaction (VIII)). In fact, the differences in $E_{1/2}$ qualitatively correlate with the differences in onset of oxygen adsorption on comparing the waves both at different electrodes (Figs. 2 and 4) and at different pH at the same electrode (Fig. 2, (Au); Table 2). However, the shift of $E_{1/2}$ with electrode material is considerably less than with onset of oxygen adsorption, e.g., in going from Au to GC, $E_{1/2}$ changes by ca. 0.6 V (Fig. 4), while the start of oxygen adsorption changes by ca. 1.1 V (Fig. 2). This can be ascribed to other factors, e.g., to the change in k^0_{app} or Γ_0 (cf. eqn. (17)).

(3) The surface redox couples which are presumably involved in NADH oxidation at solid electrodes exhibit grossly irreversible electrochemical behavior, although, for example, the oxygen adsorption at Pt [21,23] or Au [21,22] electrodes is probably initiated by the reversible adsorption of OH species. Consequently, the irreversible NADH oxidation at solid electrodes can be expected. In fact, the reciprocal slopes of the logarithmic analysis of the anodic NADH wave (Table 2) are much higher than the reversible slope of 0.059 V, which is predicted by the equation

$$(I_l - I)I^{-1} = s_c(1 + s_c)^{-1}P^{-1}$$

derived for the reversible case from eqns. (10, 12 and 13).

However, in the irreversible case, the non-linear logarithmic analysis can be expected, due to quadratic eqn. (15). At the foot of the irreversible wave, $p \ll 1$ and $(I_l - I)I^{-1} - s_{ox}$, i.e., the reciprocal slope of the logarithmic analysis approaches $2.303RT/(1-\alpha)F$. The non-linear logarithmic analysis is observed for NADH oxidation at all three electrodes, but its reciprocal slopes do not vary too much from the values given in Table 2, which would correspond to an apparent charge–transfer coefficient α of about 0.7.

(4) In general, the half-wave potential of the NADH anodic wave may depend on the electrode rotation speed, NADH concentration and solution pH (cf. eqns. (14 and 17)). In the reversible case (eqn. (14)), only the effect of the solution pH should be observed, $\Delta E^{rev}_{1/2}/\Delta\text{pH} = -2.303RT/F$, while $(\Delta E^{rev}_{1/2}/\Delta \log c^0_{NADH}) = \Delta E^{rev}_{1/2}/\Delta \log \omega = 0$. On the other hand, for the irreversible case, $\Delta E^{irr}_{1/2}/\Delta\text{pH} = 0$, while $\Delta E^{irr}_{rev}/\Delta \log \omega = 2.303RT/2F(1-\alpha)$ and $\Delta E^{irr}_{1/2}/\Delta \log c^0_{NADH} = 2.303RT/F(1-\alpha)$.

If α is assumed to be 0.7, the effects observed on NADH oxidation at Pt and Au

electrodes point to the quasi-reversible behavior of the surface redox couple, with the exception of the effect of the electrode rotation speed which corresponds rather to the behavior of an irreversible mediator redox system.

ACKNOWLEDGMENT

The authors thank the National Science Foundation which helped support the work described.

REFERENCES

1 A.L. Underwood and R.W. Burnett in A.J. Bard (Ed.), Electroanalytical Chemistry, Vol. 5, Marcel Dekker, New York, 1972, Ch. 1.
2 F.J. Elving, C.O. Schmakel and K.S.V. Santhanam, Crit. Revs. Anal. Chem., 6 (1976) 1.
3 P.J. Elving in G. Milazzo (Ed.), Topics in Bioelectrochemistry and Bioenergetics, Wiley-Interscience, 1976, Vol. I, p. 278.
4 H. Jaegfeldt, J. Electroanal. Chem.,110 (1980) 295.
5 P.J. Elving, W.T. Bresnahan, J. Moiroux and Z. Samec, Bioelectrochem. Bioenerg., 7 (1980) 125.
6 J.N. Burnett and A.L. Underwood, Biochemistry, 4 (1965) 2060.
7 R.D. Braun, K.S.V. Santhanam and P.J. Elving, J. Am. Chem. Soc., 97 (1975) 2591.
8 W.J. Blaedel and R.A. Jenkins, Anal. Chem., 47 (1975) 1337.
9 H. Jaegfeldt, A. Torstensson and G. Johansson, Anal. Chim. Acta, 97 (1978) 22.
10 M. Aizawa, R.N. Coughlin and M. Charles, Biochem. Biophys. Acta, 385 (1975) 362.
11 W.J. Blaedel and R.G. Haas, Anal. Chem. 42 (1970) 918.
12 J. Moiroux and P.J. Elving, J. Am. Chem. Soc., 102 (1980) 6533.
13 M.A. Jensen, Ph.D. Thesis, University of Michigan, Ann Arbor, 1977.
14 J. Moiroux and P.J. Elving, Anal. Chem., 50 (1978) 1056.
15 J. Moiroux and P.J. Elving, Anal. Chem., 51 (1979) 346.
16 J. Moiroux and P.J. Elving, J. Electroanal. Chem., 102 (1979) 93.
17 D.C. Tse and T. Kuwana, Anal. Chem., 50 (1978) 1056.
18 H. Jaegfeldt, A.B.C. Torstensson, L.G.O. Gorton and G. Johansson, Anal. Chem., 53 (1981) 1979.
19 D.A. Hall and P.J. Elving, Anal. Chim. Acta, 39 (1967) 141.
20 D. Jaim and W. Vielstich, J. Electrochem. Soc., 109 (1962) 849.
21 R. Woods in A.J. Bard (Ed.), Electroanalytical Chemistry, Vol. 9, Marcel Dekker, New York, 1976, p. 1.
22 M. Sotto, J. Electroanal. Chem., 72 (1976) 287.
23 B.V. Tilak, B.E. Conway and H. Angerstein-Kozlowska, J. Electroanal. Chem., 48 (1973) 1.
24 W. Böld and M. Breiter, Electrochim. Acta, 9 (1964) 1025.
25 H. Angerstein-Kozlowska and B.E. Conway, J. Electroanal. Chem., 95 (1979) 1.
26 A.A. Michri, A.G. Pshchenichnikov and R.Kh. Burshtein, Soviet Electrochem., 8 (1972) 351.
27 T. Biegler, D.A.T. Rand and R. Woods, J. Electroanal. Chem., 29 (1971) 269.
28 D.A.J. Rand and R. Woods, J. Electroanal. Chem., 35 (1972) 209.
29 K. Takamura, A. Mori and F. Kusu, Bioelectrochem. Bioenerg., 8 (1981) 229.
30 CPK Precision Molecular Models, The Ealing Corp., 2225 Massachusetts Ave., Cambridge, MA. 02140, U.S.A.
31 Z. Samec and J. Weber, Electrochim. Acta, 20 (1975) 403.
32 R.W. Murray, Acc. Chem. Res., 13 (1980) 135.
33 C.P. Andrieux, J.M. Dumas-Bouchiat and J.M. Savéant, J. Electroanal. Chem., 123 (1981) 171
34 R.R. Dogonadze, in N.S. Hush (Ed.), Reactions of Molecules at Electrodes Wiley–Interscience, New York, 1971, p. 135.